Physica Medica 140 (2025) 105677

Contents lists available at ScienceDirect

Physica Medica

journal homepage: www.elsevier.com/locate/ejmp

Bladder surface-based analysis proves the advantages of online adaptive radiotherapy over plan of the day

Sonia Sapignoli [a,1], Andrea Bettinelli [a,1], Paolo Caricato [a,*], Antonio Giuseppe Amico [a], Samuele Cavinato [a], Paola Ceroni [a], Federica Guida [a], Nicola Pivato [a], Chiara Paronetto [b], Badr Elkhouzai [b], Matteo Sepulcri [b], Marco Krengli [b], Marta Paiusco [a]

[a] Medical Physics Department, Veneto Institute of Oncology IOV - IRCCS, Padua, Italy
[b] Radiation Oncology Department, Veneto Institute of Oncology IOV - IRCCS, Padua, Italy

ARTICLE INFO

Keywords:
Bladder cancer
Adaptive radiotherapy
Plan of the Day
Online Adaptive Radiotherapy
Dose-Surface Histogram
Surface Distance Histogram

ABSTRACT

Background: Radiotherapy delivery for bladder cancer is challenging due to inter- and intra-fraction anatomical variations. The literature shows that surface-based methods, such as cumulative Dose-Surface Histograms (cDSHs), are more appropriate than dose-volume histograms for evaluating dose distribution in hollow organs.
Purpose: To compare two adaptive radiotherapy approaches – Plan of the Day (POD) and online-Adaptive Radiotherapy (oART) – by focusing on target coverage, dose conformity, and healthy tissue sparing through surface-based methods.
Methods: Five patients with urothelial bladder cancer were selected. POD and oART treatment (9-field-IMRT plans, 55 Gy/20 fractions) were simulated using the Ethos™ Emulator.
The cDSHs were compared using the D98% and D50% metrics, describing the dose covering 98% and 50% of the PTV/CTV surface, respectively. The Surface Distance Histogram (SDH) was introduced and analysed through Full Width at Half Maximum and mode value. The Healthy Tissue Overdose volume Factor (HTOF) at 95% and 50% isodoses was calculated. Statistical comparisons included the Friedman test and the Canberra dissimilarity index.
Results: oART achieved superior PTV coverage, with a mean D98% consistently above 98% of the prescribed dose, whereas for POD, the mean D98% dropped below 90% for two patients. oART SDHs showed narrower bell shape with respect to POD, indicating higher dose conformity. oART improved healthy tissue sparing, reducing $HTOF_{95\%}$ by over 50% compared to POD. Inter- and intra-patient variability were lower for oART.
Conclusions: Surface analysis strengthens the notion that oART is advantageous in bladder cancer treatment, ensuring superior target coverage, enhanced dose conformity, and better healthy tissue sparing. The SDH findings suggest potential for reducing CTV-PTV margins.

1. Introduction

Radiotherapy delivery for bladder cancer presents unique challenges due to inter- and intra- fraction variations in bladder filling, rectal distension, and bowel motion. These changes can compromise target coverage and increase toxicity to healthy tissues [1–3], thus there is a pressing need for advanced treatment strategies to increase accuracy and minimise side effects. Adaptive radiotherapy (ART) techniques have been introduced to address these issues, allowing adjustments in treatment plans to account for daily anatomical variations.

A commonly used ART strategy is the Plan of the Day (POD), where daily imaging is used to select the best fitting plan from a library of patient-specific plans pre-calculated for different bladder fillings [4–6].

Another approach, online-Adaptive Radiotherapy (oART), involves the daily treatment plan re-optimization according to the cone-beam computed tomography (CBCT) or magnetic resonance (MR) images acquired before the treatment [7–10].

The potential benefit of ART over conventional radiotherapy for bladder treatment [7,8,10–13], has been shown by several studies and dose-volume histograms (DVHs) are commonly used to assess the quality of the planning.

However, given that the bladder is a hollow organ, the DVH may not

* Corresponding author.
E-mail address: paolo.caricato@iov.veneto.it (P. Caricato).
[1] The authors contributed equally to this work.

https://doi.org/10.1016/j.ejmp.2025.105677
Received 13 March 2025; Received in revised form 24 July 2025; Accepted 13 November 2025
Available online 22 November 2025

be the optimal descriptor of the dose delivered to the target, as the dose to the content is not relevant. In a case of empty organs, the Dose-Wall Histogram (DWH) or the cumulative Dose-Surface Histogram (cDSH) are suggested as more appropriate tools [14–17].

Based on the above, the aim of the study was to compare the POD and oART strategies by focusing on the bladder surface. These two approaches were evaluated in term of cDSH, which was used to evaluate the target coverage, and the differential Surface Distance Histogram (SDH) [18] which was introduced to estimate the dose conformity.

2. Materials and methods

2.1. Patient population

Five patients with cT2 cN0 urothelial bladder cancer, three males and two females, treated with the POD technique, were included in the study. The entire volume of the bladder was delineated as the clinical target volume (CTV), with an isotropic margin of 0.7 cm added to create the planning target volume (PTV). The small bowel, femoral heads, and uterus/prostate were delineated as organs at risk (OARs). All patients were prescribed to a total dose of 55 Gy in 20 fractions to the PTV, with planning objectives of PTV D98% > 95% and PTV D2% < 105%.

At our institution, the POD protocol involves acquiring three planning CT (pCT) scans: the first with empty bladder, followed by two subsequent scans performed at 15 and 30–40 min after patients' consumption of 500 ml of water. A library of three treatment plans, P_{empty}, P_{mid}, and P_{full}, corresponding to the time markers, was created. Volumetric Modulated Arc Therapy (VMAT) plans, two 6 MV arcs, were generated with Eclipse v16.1 – AcurosXB algorithm (Varian Medical Systems, Inc., Palo Alto, CA). For each treatment session, a CBCT image was acquired on a TrueBeam STX linac (Varian Medical Systems, Inc., Palo Alto, CA) and the best fitting plan was selected from the pre-calculated library.

2.2. Treatment emulation

Recently, the Ethos™ Therapy system [19] (Varian Medical Systems, Inc., Palo Alto, CA), an advanced linear accelerator designed to provide both Image-Guided Radiotherapy (IGRT) and oART, was installed at our institute. Additionally, the 'Ethos Emulator' [20], a related research platform replicating the entire Ethos™ workflow, from treatment planning to delivery, was also installed. Therefore, to facilitate a comparative analysis of POD and oART plans under consistent conditions (same Intelligent-Optimization-Engine (IOE), geometry and delivery technique), both approaches were simulated using Ethos Emulator. Below, we detail the operational processes used for the simulation (a diagram of the workflow is shown in Fig. S1). The first step was 'Treatment preparation': the three clinical pCTs and related structure sets were imported into the Emulator from ARIA (Varian Medical Systems); the 'Physician Intent' was established, which involves defining the diagnosis, treatment prescriptions (55 Gy in 20 fractions), target volumes, and OARs; a list of prioritised clinical goals was defined for dose optimization and applied to both POD and oART (reported in Table S1); three 9-field intensity modulated radiation therapy (IMRT) plans (i.e., P_{empty}, P_{mid}, and P_{full}), serving as reference plans (RPs) within the Ethos framework, were generated for each corresponding pCT. IMRT was selected over VMAT due to its shorter Ethos computation time, with 9-field IMRT plans generated in approximately 2.5 min, compared to 13 min for VMAT plans. This choice kept the total adaptive treatment duration comparable to that of POD treatments, approximately 15 and 12 min, respectively and allowed us to adopt the same 7 mm margin utilized in our institutional POD strategy. The resulting RPs were approved by a physicist and a radiation oncologist expert in bladder treatment.

As a second step we performed the 'Daily online treatment', in which the daily CBCT image of the clinical treatments was fed into the Emulator to simulate the actual daily scan and to generate the daily synthetic CT (sCT) scan; the radiation oncologist reviewed and edited, when necessary, the automated AI-driven OAR contouring. To replicate the POD treatment, for each session the best-fitting RP was selected and automatically recalculated on the sCT scan while, for oART simulation, the P_{mid} was always used as RP plan with the related re-optimized adaptive dose distribution approved by the radiation oncologist.

2.3. Analysis

2.3.1. Surface creation and sampling strategy

For both the CTV and PTV, DICOM slice-by-slice contours were converted into binary masks using the crossing number algorithm. Surface meshes were then generated using the marching cubes algorithm and smoothed with a dedicated MATLAB package (MATLAB R2021a; The MathWorks, Inc., Natick, MA, USA) [21], as shown in Fig. 1a, left. Isodose surfaces at 50 % and 95 % ($ISO_{50\%}$ and $ISO_{95\%}$) levels were obtained from the 3D dose distribution using the MATLAB 'isosurface' function (1a, right).

To sample the surfaces in all 3D directions from a reference point (O), specifically the centre of mass of the target volume (either PTV or CTV), we employed directions determined by the radial segments extending from O to the vertices of a subdivided icosahedron centred on O. Specifically, a 32-frequency subdivided icosahedron with $N = 10,242$ vertices was generated as a primitive mesh in Blender 2.90.1 (Blender Institute, Amsterdam, The Netherlands) and subsequently imported into MATLAB for use in the sampling procedure. This approach allows the systematic sampling of the space with nearly equal solid angles. The coordinates of the sampling points were determined by finding the intersections between the sampling directions and the surface of interest (CTV/PTV/isodose), see Supplementary Fig. S2a. This method ensures consistent sampling across different surfaces, facilitating direct comparisons between them, and produces triangular meshes.

2.3.2. Surface dose extraction and isodose distance calculation

To determine the dose values on the surface of the volume of interest (VOI), we sampled the entire 3D dose distribution at the coordinates of the surface vertices using trilinear interpolation (Fig. 1b).

The distances between surfaces were computed on a point-by-point basis (Fig. 1c). Let $d_n^{iso} = |\overrightarrow{OI_n}|$ and $d_n^{voi} = |\overrightarrow{OV_n}|$ be the lengths of the radius vectors from the reference point O to I_n (the n^{th} vertex of the sampled $ISO_{95\%}$), and V_n (the n^{th} vertex of the sampled VOI surface, either the PTV or CTV), respectively. The N radial distances between the two surfaces were calculated as follows: $d_n = d_n^{iso} - d_n^{voi} = |\overrightarrow{OI_n}| - |\overrightarrow{OV_n}|$.

The employed sampling process allows for a 2D visualisation of both sampled doses and distances, since, by construction, the n^{th} vertices of the isodose and region of interest are one-to-one linked to the n^{th} vertex of the polyhedron surface, which can be unwrapped onto a 2D plane by converting its Cartesian coordinates to spherical coordinates.

2.3.3. Treatment evaluation tools

Target coverage was evaluated for each fraction by the cDSH, calculated for each bin i as follow:

$$cDSH_k = 1 - \sum_{j=1}^{k} \left(\frac{\sum_{n=1}^{N} \left([D_n \in b_j] \bullet w_n \right)}{N} \right) \quad (1)$$

where k ranges from 1 to K, K denotes the number of bins (180), D_n represents the dose at VOI vertex n^{th}, b_j the j^{th} bin,w_n is a normalized weighting factor (see the dedicated supplementary paragraph "Vertex weighting to account for variations in sampling density"), δ the bin width and the square brackets (Iverson brackets) equal 1 if the condition is true and 0 otherwise. The histogram represents the cumulative percentage surface area receiving a dose no less than a specified dose as a function of the defined dose (Fig. 1f).

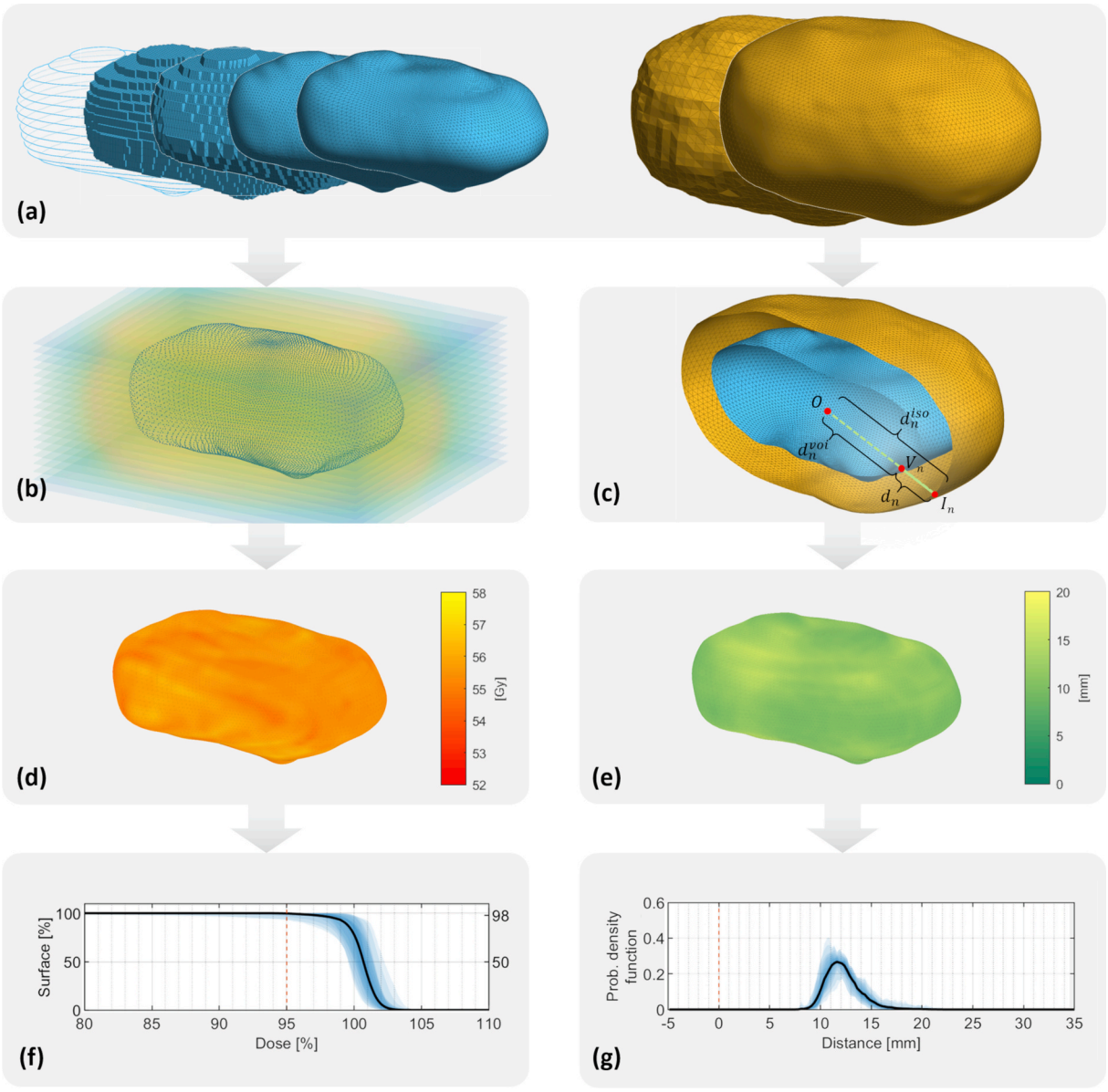

Fig. 1. Schematic overview of the methodological framework employed for the analysis. (a) Sequential representations of the volume of interest (VOI) in blue (contour set, binary mask, marching-cube surface, smoothed surface and sampled surface), and of the $ISO_{95\%}$ in orange (original and sampled surface). (b) Dose value sampling on VOI surface vertices (blue dots), (c) VOI-isodose distance calculation (O: reference point; I_n: n^{th} vertex of the sampled $ISO_{95\%}$; V_n: n^{th} vertex of the sampled VOI surface; d_n^{iso} and d_n^{voi}: n^{th} distances from VOI/$ISO_{95\%}$ to the reference point; d_n: n^{th} distance between the two surfaces). (d) Sampled VOI surface doses and (e) VOI-isosurface distances visualised on the VOI surface. (f) Cumulative dose-surface histogram and (g) surface distance histogram. (For interpretation of the references to colour in this figure legend, the reader is referred to the web version of this article.)

The dose conformity was analysed based on the differential SDH, Fig. 1g, which describe the distribution of the distances between $ISO_{95\%}$ and VOI surfaces (either PTV or CTV):

$$SDH_k = \frac{\sum_{n=1}^{N}([d_n \epsilon b_k] \bullet w_n)}{N \bullet \delta} \quad (2)$$

where d_n is the n^{th} distance between the two surfaces.

Finally, Healthy Tissue Overdose volume Factor (HTOF) [22] was used as a surrogate for the dose to the OAR. HTOF represents the volume (cm^3) of healthy tissue outside the PTV normalized to the PTV volume $HTOF_{D\%} = (V_{D\%} - V_{PTV})/V_{PTV}$, $V_{D\%}$ is the volume of the body receiving a dose greater than a $D\%$ of the prescription dose (both $D\% = 50\%$ and $D\% = 95\%$ were considered), and V_{PTV} the PTV volume. $HTOF_{D\%}$ is normalised to consider the variability in inter-fraction bladder volume. A $HTOF_{D\%}$ of zero means that normal tissue does not receive a dose higher than the selected threshold.

2.3.4. Statistical analysis

To compare the cDSHs of the ART strategies under consideration, two representative dose points metrics were selected: D98% and D50%, describing the doses covering 98% and 50% of the surface, respectively.

The non-parametric Friedman test was used to assess differences in D98% and D50% across the two techniques in a repeated-measures design. Each subject served as its own control, and repetitions corresponded to the 20 fractions. A significance level of $\alpha = 0.05$ was considered statistically significant.

The SDHs were described in terms of Full Width at Half Maximum (FWHM) and mode value. The non-parametric Friedman test was again applied to evaluate differences in both SDH metrics.

The SDHs were also compared by means of the Canberra dissimilarity

metric [23]:

$$C_{AB} = \frac{1}{K}\sum_{k=1}^{K}\frac{|SDH_k^A - SDH_k^B|}{|SDH_k^A| + |SDH_k^B|} \quad (3)$$

where A and B were set to compute the Canberra metric between patients (e.g., A = patient 1 POD and B = patient 2 POD) or between techniques (e.g., A = patient 1 POD and B = patient 1 oART), and K the numbers of bins.

The Friedman test was used to analyse statistically significant differences in $HTOF_{95\%}$ and $HTOF_{50\%}$ for POD and oART, using the same approach as described earlier. Statistical analysis was performed with MATLAB.

3. Results

For the POD approach, P_{empty}, P_{mid}, P_{full} were selected 12, 74 and 14 times out of the 100 simulated fractions, respectively.

The inter-fraction variation of the bladder volume is shown in Fig. 2a. Large inter-fraction bladder volume variations were observed in 3 of the 5 patients, with bladder volume more than doubling across some sessions. Given these volumes, we estimated that CTV and PTV surfaces were sampled, on average, with point spacing of 0.96 mm and 1.26 mm, respectively.

Fig. 3 presents, for each patient, the average cDSH for the PTV (CTV in Fig. S4), with blue bands representing the density intervals of the cDSH across all fractions. Table 1 reports both mean and standard deviation of D98% and D50% calculated for each patient across all fractions. oART exhibited narrower bands compared to POD, as also indicated by D95% and D98% standard deviation values. Additionally, oART provided optimal PTV coverage, with an average D98% dose consistently higher than 98% of the prescribed dose, while for POD there were cases where the average dose was less than 90% of the prescribed dose. However, despite POD low performances for PTV surface coverage, 98% of CTV surface always received at least 95% of the prescribed dose (Fig. S4). Fig. 4 reports exemplifying unwrapped dose surface maps (all maps can be found in an online Zenodo repository [24]: despite the PTV surface being underdosed, the CTV remained covered. The Friedman test revealed significant ($p < 0.001$) differences for PTV in both D98% and D50% between oART and POD, while for the CTV, significant differences were observed only for D98%.

Fig. 5 shows the PTV SDH and Table 2 reports the mean and standard deviation of the FWHM and mode of the SDH, calculated for each patient across all fractions. The oART distributions have a narrower bell shape with respect to the POD distributions, which in turn are wider and more dispersed (see FWHM in Table 2). The extreme values of the POD SDH reached distances larger than 1 cm from the PTV surface. A similar behaviour was observed for the CTV SDHs (Fig. S5).

It is interesting to note that, for the PTV, the lower limits of oART SDH were never below zero.

The Friedman test revealed significant ($p < 0.001$) differences between treatment modalities for both FWHM and mode, both for PTV and CTV. The differences between POD and oART are corroborated by the Canberra index. When comparing pairwise the SDH of the PTV for the two treatment modalities, the Canberra index exceeded 0.5 for each patient, with a mean value of 0.62. However, when comparing histograms pairwise among patients for a fixed modality, the value consistently fell below 0.5 for oART (see Fig. S3 for all values).

Fig. 2b-c shows the $HTOF_{95\%}$ and $HTOF_{50\%}$ for each patient and fraction. Improved healthy tissue sparing is observed with oART

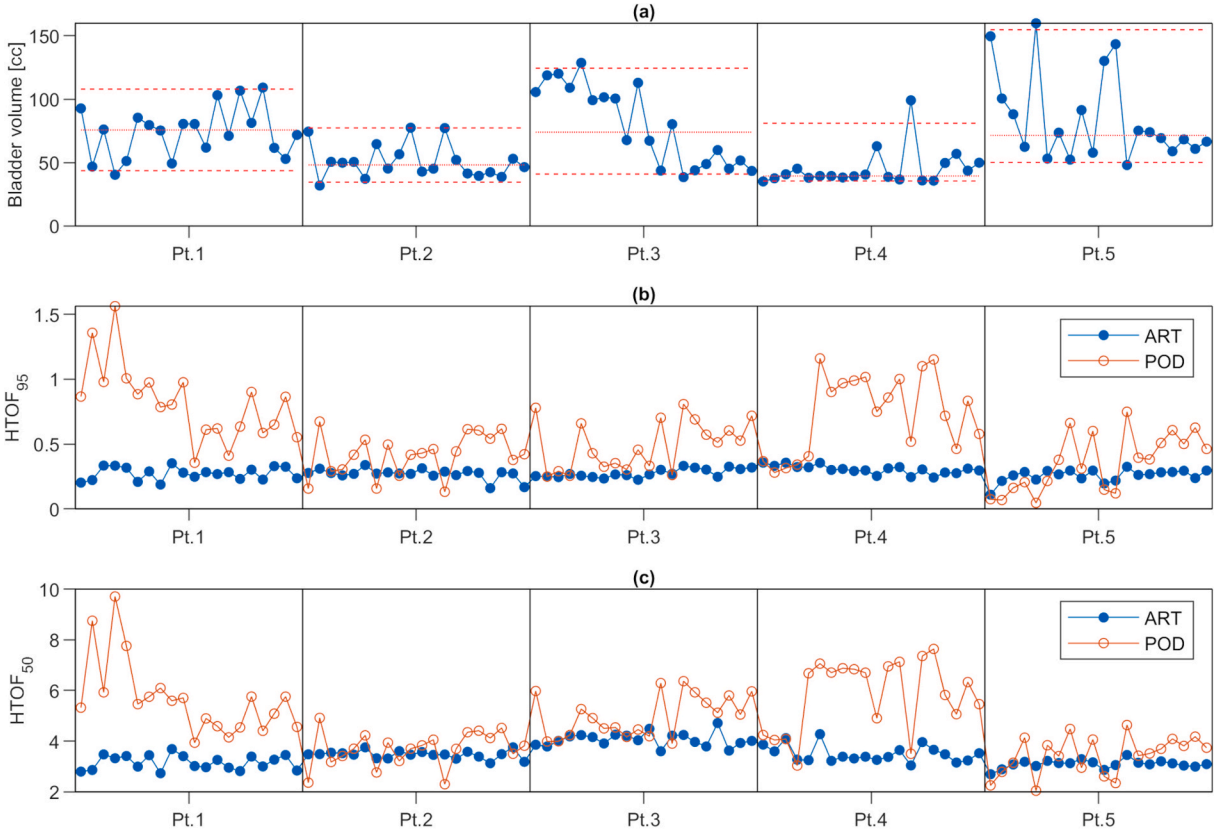

Fig. 2. (a) Bladder volume variations for each fraction and each patient. The dashed lines indicate the 5th-95th percentile range, while the solid line the median bladder volume, both calculated individually for each patient. (b-c) Normalised healthy tissue volumes receiving (b) 95% and (c) 50% of the prescribed dose per fraction across the entire dataset for both oART (red) and POD (blue) approaches. (For interpretation of the references to colour in this figure legend, the reader is referred to the web version of this article.)

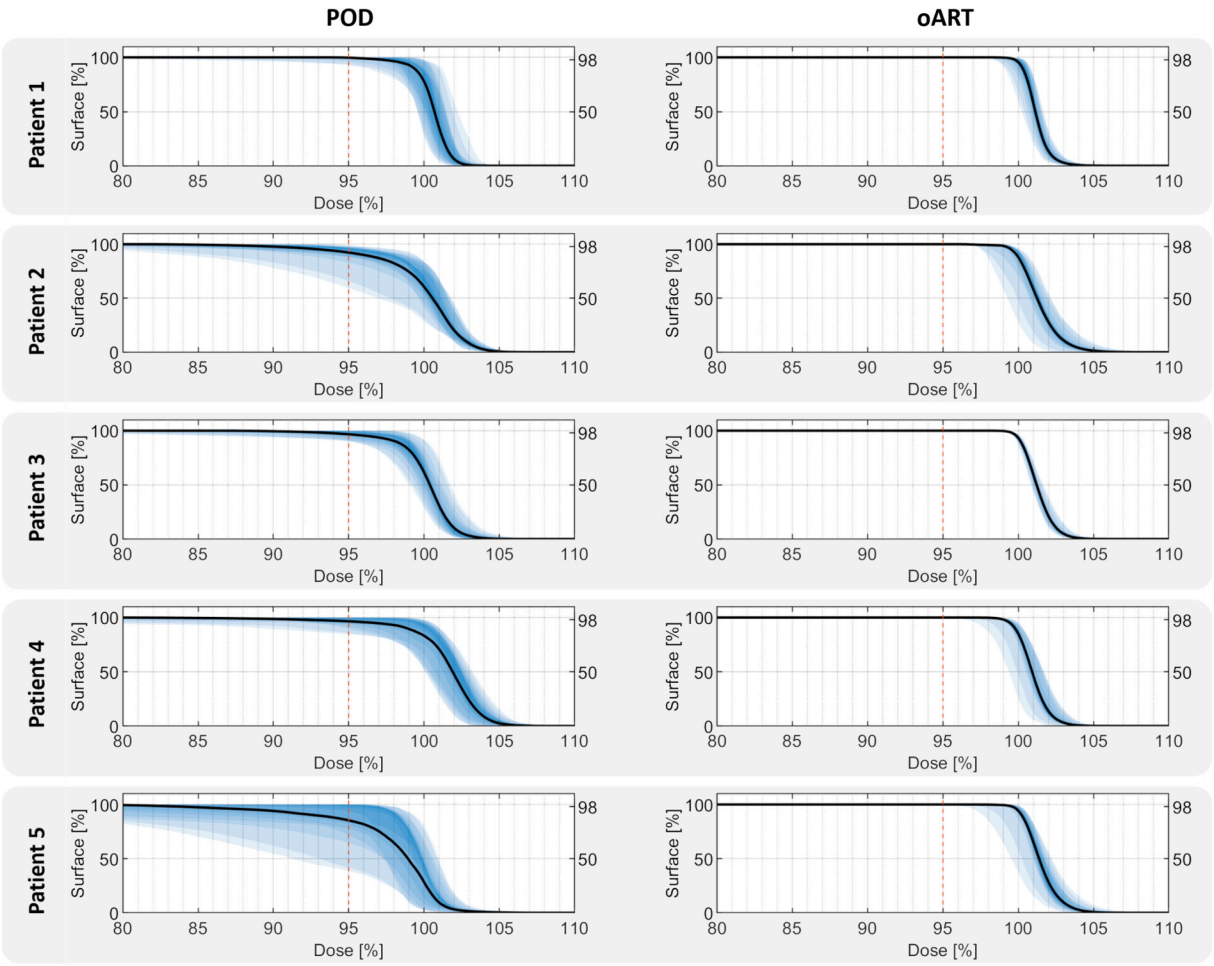

Fig. 3. Mean (black curves) PTV cumulative Dose-Surface Histogram (cDSH) for POD (left) and oART (right). The blue bands represent density intervals of the cDSH at increasing inter-percentile ranges (from 0% to 100% in 5% increments) across all fractions. The red dashed line represents the 95% of prescribed dose. (For interpretation of the references to colour in this figure legend, the reader is referred to the web version of this article.)

Table 1
Mean and standard deviation of all cDSHs calculated at 98% and 50% of the surface (D98% and D50%) for both simulated treatment modalities. Results are shown for both PTV and CTV.

		PTV		CTV	
		POD	**oART**	**POD**	**oART**
D98%					
	Pt. 1	97.1 ± 3.9	99.7 ± 0.6	99.1 ± 0.9	100.0 ± 0.3
	Pt. 2	89.5 ± 6.4	99.1 ± 0.7	99.0 ± 0.7	99.4 ± 0.4
	Pt. 3	93.5 ± 6.2	99.6 ± 0.2	99.0 ± 0.9	99.6 ± 0.1
	Pt. 4	91.9 ± 13.6	99.1 ± 0.6	99.9 ± 0.8	99.4 ± 0.3
	Pt. 5	83.9 ± 21.4	99.6 ± 0.8	97.7 ± 1.2	99.9 ± 0.2
D50%					
	Pt. 1	100.7 ± 0.8	101.1 ± 0.3	100.3 ± 0.8	100.7 ± 0.2
	Pt. 2	100.6 ± 1.2	101.2 ± 0.6	100.8 ± 0.6	100.5 ± 0.4
	Pt. 3	100.4 ± 0.6	101.2 ± 0.2	100.5 ± 0.7	100.4 ± 0.2
	Pt. 4	101.9 ± 1.0	100.9 ± 0.5	101.6 ± 0.9	100.2 ± 0.4
	Pt. 5	98.9 ± 2.3	101.4 ± 0.6	99.2 ± 0.8	100.7 ± 0.2

modality compared to POD. The Friedman test demonstrates that the differences with POD are statistically significant ($p < 0.001$).

4. Discussions

This study compared Plan of the Day (POD) with on-line Adaptive Radiotherapy (oART) for the treatment of bladder cancer by a surface-based analysis. The results showed that oART outperforms POD in terms of target coverage, dose conformity, reduces intra- and inter-patient variability and also improves healthy tissue sparing.

Concerning target coverage, the cDSHs (Fig. 3 and Table 1) show that oART ensured at least 95% of the prescribed dose to 98% of the PTV surfaces across all 100 treatment sessions, resulting in CTV surfaces that were always covered by more than the 98% of the dose. The same cannot be said for POD, where for each patient, at least one fraction delivered 95% of the dose to less than 98% of the PTV surfaces, and in some cases, this coverage fell below 90%. However, both ART modalities ensured that at least 95% of the prescribed dose covered 98% of the CTV surface (Fig. S4). In this regard, the dose maps obtained from the unwrapped dose surface is emblematic. Fig. 4 shows the maps for the 7th fraction of patient #2, where PTV surface showed significant underdosing (dose below 95% in the central area of the map), in contrast, the CTV was covered by 98% of the prescribed dose.

The SDHs (Fig. 5) also contain the previously described results on target coverage. Indeed, oART $ISO_{95\%}$ surfaces always enveloped the PTV, since reported distances were always positive. On the other hand, for POD, the distances were also distributed on negative values indicating that the $ISO_{95\%}$ interpenetrated the PTV surface, compromising target coverage.

In accordance with other studies [8,11], our results confirm that the on-line technique performs better than POD in dose conformation: Fig. 5 shows that for the oART technique the $ISO_{95\%}$ exceeds PTV by

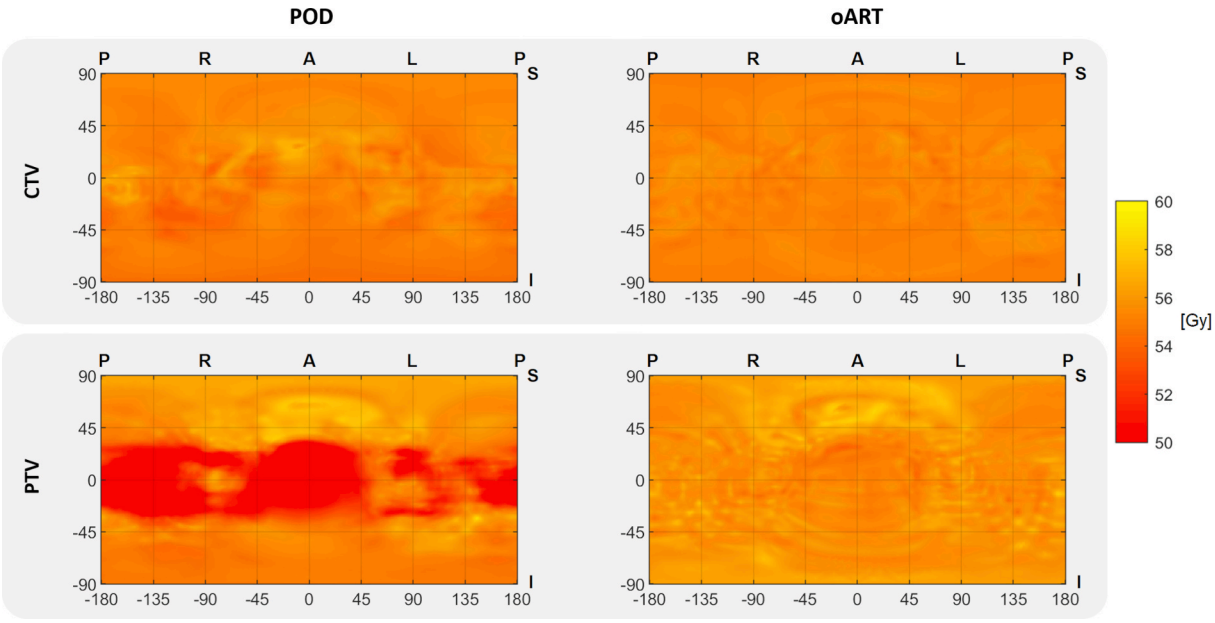

Fig. 4. The dose-surface maps of the 7th fraction of patient #2. The PTV surface in the POD plan is underdosed in its central region, while the oART plan guarantees an adequate dose coverage to both PTV and CTV. A: anterior, P: posterior, R: right, L = left, S = superior, I = inferior.

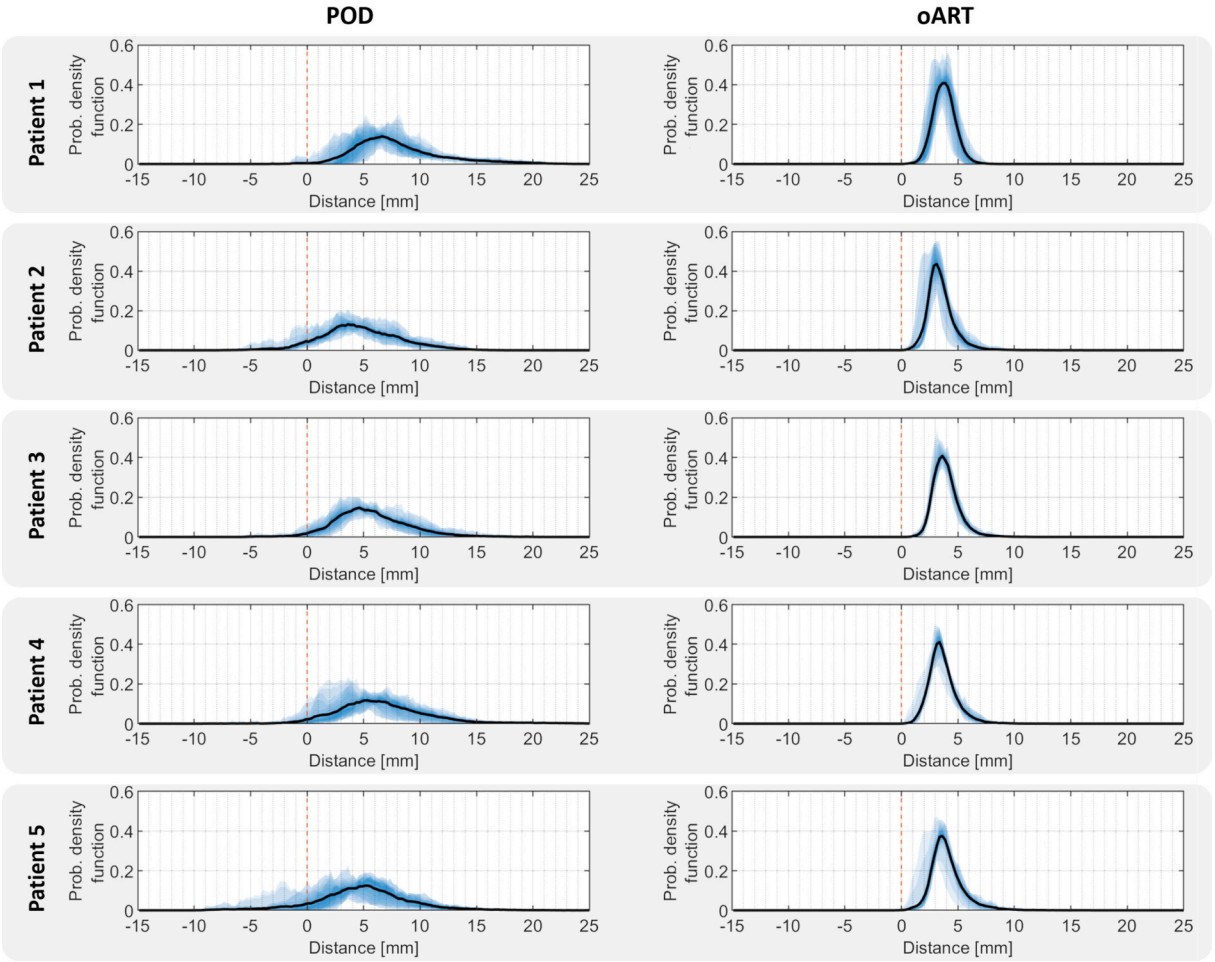

Fig. 5. Mean (black curves) $ISO_{95\%}$-PTV Surface Distance Histograms (SDHs) for each patient for POD (left) and oART (right) approaches. The red dashed lines separate negative (no coverage) and positive (coverage) distances. The blue bands represent density intervals of the SDH at increasing inter-percentile ranges (from 0% to 100% in 5% increments) across all fractions. (For interpretation of the references to colour in this figure legend, the reader is referred to the web version of this article.)

Table 2
Mean and standard deviation of FWHM and mode of the SDH for both simulated treatment modalities. Results are shown for both PTV and CTV.

		PTV		CTV	
		POD	oART	POD	oART
Pt. 1	FWHM [mm]	4.16 ± 1.17	1.90 ± 0.33	4.36 ± 1.18	2.84 ± 0.49
	Mode [mm]	6.10 ± 1.63	3.72 ± 0.59	13.76 ± 1.88	11.79 ± 0.73
Pt. 2	FWHM [mm]	5.64 ± 1.89	1.73 ± 0.36	7.59 ± 1.66	2.93 ± 0.54
	Mode [mm]	3.73 ± 1.76	3.00 ± 0.34	12.43 ± 1.97	11.20 ± 0.53
Pt. 3	FWHM [mm]	5.40 ± 1.06	1.94 ± 0.29	6.34 ± 1.54	3.43 ± 0.87
	Mode [mm]	5.38 ± 1.54	3.65 ± 0.29	13.80 ± 1.64	12.17 ± 0.70
Pt. 4	FWHM [mm]	5.27 ± 1.43	1.92 ± 0.34	6.30 ± 1.79	2.82 ± 0.46
	Mode [mm]	5.48 ± 1.53	3.27 ± 0.19	13.92 ± 1.82	11.35 ± 0.43
Pt. 5	FWHM [mm]	4.89 ± 1.22	1.98 ± 0.26	6.42 ± 2.36	3.60 ± 1.04
	Mode [mm]	3.75 ± 2.29	3.57 ± 0.34	12.38 ± 2.75	11.63 ± 0.56

approximately 5 mm while for the Plan of the Day it extends to distances even beyond 1 cm.

These findings are closely related to the intrinsic characteristics of the two adaptive modalities [7,12], In the POD strategy, the plan is chosen fraction by fraction from the library of plans generated for three different bladder fillings. However, the bladder not only changes in volume but also in shape and position due to daily variations in the internal anatomy. Therefore, in the POD technique, the delivered plan should be a trade-off between CTV coverage and healthy tissue dose, sometimes compromising the PTV coverage. In contrast, variations in shape and position are effectively managed with oART, as treatment is re-planned based on daily anatomical changes, applying the same 'planning target list' (Table S1) and a 7 mm margin around the CTV.

Re-planning based on daily anatomy minimizes both inter- and intra-patient variability. The Ethos −oART plans demonstrate high similarity, as evidenced by the standard deviations of both D98% and D50% ($p < 0.001$), along with consistent means for PTV mode and FWHM across all patients (Table 2). Additionally, the Canberra metric, which assesses pairwise comparisons among patients for a fixed modality, consistently remains below 0.5 (with an average of 0.3). This further emphasises the robustness of the Ethos solutions in terms of patient variability.

It is noteworthy that the lower limit of the $ISO_{95\%}$-PTV is always zero. This underlines that Ethos always respects the assigned margin, thereby ensuring excellent PTV coverage, almost as if it were a hard constraint. The optimizer's capacity to maintain this margin suggests that, at least in this clinical context, there may be potential to safely reduce the margin.

The effectiveness of oART compared to the POD strategy is particularly relevant in healthy tissues sparing, as previously reported [7,8,11]. As shown in Fig. 2b, both $HTOF_{95\%}$ and $HTOF_{50\%}$, for oART technique, remained consistent for each fraction and patient: information implicitly included in the similarity of the SDHs. $HTOF_{95\%}$ of oART technique is, on average, 0.70 times that of POD, indicating a tissue saving of approximately 30%.

The lower performance of POD in tissue sparing is strictly related to the impossibility to take into account variations in shape and position, an intrinsic limit that, as stated before, forces a compromise between target coverage and irradiated healthy tissue. Evidence of this is patient 4 in Fig. 2a, where we observed that in the first 10 fractions, despite the volume being relatively constant, the irradiated healthy tissue greatly varies.

As in previous ART studies [8,11,25], the work conducted on the basis of inter-fraction variations inferred from pre-treatment CBCT. However, to reduce the margin—a potentially achievable objective due to the performance of the Ethos optimizer— it is essential to incorporate post-treatment CBCT in future studies. This would allow for a comprehensive assessment of residual errors attributable to intra-fraction variability. Additionally, the prolonged treatment times inherent to ART strategies may introduce variations in bladder filling. This variability is patient-specific and influenced by the hydration protocols employed [26]. Consequently, it is crucial to consider these factors not only in the selection of ART strategies but also in the definition of treatment margins.

5. Conclusions

This study proves that the oART approach significantly outperforms the POD method for bladder cancer treatment. The use of surface-based analysis, such as cDSH and SDH, demonstrated its ability to enhance target coverage, consistently conform the dose to the target, minimise healthy tissue exposure to high radiation doses, and reduce the intra- and inter-patient variability. Furthermore, the findings suggest potential for reduced CTV-to-PTV margins in oART treatment, which could in turn reduce the risk of gastrointestinal toxicity.

Declaration of competing interest

The authors declare that they have no known competing financial interests or personal relationships that could have appeared to influence the work reported in this paper.

Acknowledgments

This work received 'Ricerca Corrente 2025' funding from the Italian Ministry of Health to cover publication costs.

Authorship

The authors' contributions are as follows: SS, AB, PCA, and MP contributed to the conception and design of the study; SS, PCA, AGA, PCE, FG, and NP contributed to the acquisition of data; SS, AB, PCA, SC, and MP contributed to the analysis and interpretation of data; SS, AB, PCA, and MP contributed to drafting the article; AGA, PCE, FG, CP, BE, MS, and MK contributed to critically revising it for important intellectual content. All authors contributed to the final approval of the version to be submitted.

Declaration of generative AI and AI-assisted technologies in the writing process

During the preparation of this work the author(s) used ChatGPT-3.5 and DeepL Write in order to check the spelling and improve the legibility of the text. After using this tool/service, the author(s) reviewed and edited the content as needed and take(s) full responsibility for the content of the publication.

Appendix A. Supplementary data

Supplementary data to this article can be found online at https://doi.org/10.1016/j.ejmp.2025.105677.

Data availability

The dataset presented in this study can be found in the online Zenodo repository (doi: 10.5281/zenodo.14593384).

References

[1] Muren LP, Smaaland R, Dahl O. Organ motion, set-up variation and treatment margins in radical radiotherapy of urinary bladder cancer. Radiother Oncol 2003; 69(3):291–304. https://doi.org/10.1016/S0167-8140(03)00246-9.

[2] Pos FJ, Koedooder K, Hulshof MCCM, Van Tienhoven G, González González D, Koedooder C. Influence of bladder and rectal volume on spatial variability of a bladder tumor during radical radiotherapy. Int J Radiat Oncol Biol Phys 2003;55 (3):835–41. https://doi.org/10.1016/S0360-3016(02)04158-5.

[3] Dees-Ribbers HM, Betgen A, Pos FJ, Witteveen T, Remeijer P, Van Herk M. Inter- and intra-fractional bladder motion during radiotherapy for bladder cancer: a comparison of full and empty bladders. Radiother Oncol 2014;113(2):254–9. https://doi.org/10.1016/J.RADONC.2014.08.019.

[4] Foroudi F, Wong J, Kron T, et al. Online adaptive radiotherapy for muscle-invasive bladder cancer: results of a pilot study. Int J Radiat Oncol Biol Phys 2011;81(3): 765–71. https://doi.org/10.1016/j.ijrobp.2010.06.061.

[5] Lutkenhaus LJ, Visser J, De Jong R, Hulshof MCCM, Bel A. Evaluation of delivered dose for a clinical daily adaptive plan selection strategy for bladder cancer radiotherapy. Radiother Oncol 2015;116(1):51–6. https://doi.org/10.1016/j.radonc.2015.06.003.

[6] den Boer D, den Hartogh MD, Kotte ANTJ, et al. Comparison of Library of Plans with two daily adaptive strategies for whole bladder radiotherapy. Phys Imaging Radiat Oncol 2021;20:82–7. https://doi.org/10.1016/J.PHRO.2021.11.002.

[7] Vestergaard A, Muren LP, Søndergaard J, Elstrøm UV, Høyer M, Petersen JB. Adaptive plan selection vs. re-optimisation in radiotherapy for bladder cancer: a dose accumulation comparison. Radiother Oncol 2013;109(3):457–62. https://doi.org/10.1016/J.RADONC.2013.08.045.

[8] Åström LM, Behrens CP, Calmels L, et al. Online adaptive radiotherapy of urinary bladder cancer with full re-optimization to the anatomy of the day: initial experience and dosimetric benefits. Radiother Oncol 2022;171:37–42. https://doi.org/10.1016/J.RADONC.2022.03.014.

[9] Davis R, Ladbury C, Tsai K, et al. CT-guided online adaptive hypofractionated radiotherapy for primary bladder cancer: a report of two cases. Cureus 2024;16(8). https://doi.org/10.7759/CUREUS.67318.

[10] Mitchell A, Ingle M, Smith G, et al. Feasibility of tumour-focused adaptive radiotherapy for bladder cancer on the MR-linac. Clin Transl Radiat Oncol 2022; 35:27–32. https://doi.org/10.1016/J.CTRO.2022.04.008.

[11] Azzarouali S, Goudschaal K, Visser J, et al. Online adaptive radiotherapy for bladder cancer using a simultaneous integrated boost and fiducial markers. Radiat Oncol 2023;18(1). https://doi.org/10.1186/S13014-023-02348-8.

[12] Kong VC, Taylor A, Chung P, Craig T, Rosewall T. Comparison of 3 image-guided adaptive strategies for bladder locoregional radiotherapy. Med Dosim 2019;44(2): 111–6. https://doi.org/10.1016/J.MEDDOS.2018.03.004.

[13] Sibolt P, Andersson LM, Calmels L, et al. Clinical implementation of artificial intelligence-driven cone-beam computed tomography-guided online adaptive radiotherapy in the pelvic region. Phys Imaging Radiat Oncol 2020;17:1–7. https://doi.org/10.1016/J.PHRO.2020.12.004.

[14] Carillo V, Cozzarini C, Chietera A, et al. Correlation between surrogates of bladder dosimetry and dose-volume histograms of the bladder wall defined on MRI in prostate cancer radiotherapy. Radiother Oncol 2012;105(2):180–3. https://doi.org/10.1016/J.RADONC.2012.10.001.

[15] Palorini F, Botti A, Carillo V, et al. Bladder dose-surface maps and urinary toxicity: Robustness with respect to motion in assessing local dose effects. Phys Med 2016; 32(3):506–11. https://doi.org/10.1016/J.EJMP.2016.03.006.

[16] Hoogeman MS, Peeters STH, De Bois J, Lebesque JV. Absolute and relative dose-surface and dose-volume histograms of the bladder: which one is the most representative for the actual treatment? Phys Med Biol 2005;50(15):3589–97. https://doi.org/10.1088/0031-9155/50/15/007.

[17] Maggio A, Carillo V, Cozzarini C, et al. Impact of the radiotherapy technique on the correlation between dose-volume histograms of the bladder wall defined on MRI imaging and dose-volume/surface histograms in prostate cancer patients. Phys Med Biol 2013;58(7). https://doi.org/10.1088/0031-9155/58/7/N115.

[18] Diamantopoulos S, Platoni K, Karaiskos P, Kouloulias V, Efstathopoulos E. Isodose surface differences: a novel tool for the comparison of dose distributions. J Appl Clin Med Phys 2023;24(11). https://doi.org/10.1002/ACM2.14085.

[19] Archambault Y, Boylan C, Bullock D, et al. Making on-line adaptive radiotherapy possible using artificial intelligence and machine learning for efficient daily re-planning. Med Phys Int J 2020;8(2):77–86.

[20] Moazzezi M, Rose B, Kisling K, Moore KL, Ray X. Prospects for daily online adaptive radiotherapy via ethos for prostate cancer patients without nodal involvement using unedited CBCT auto-segmentation. J Appl Clin Med Phys 2021; 22(10):82–93. https://doi.org/10.1002/ACM2.13399.

[21] Marc Lalancette. SurfaceSmooth. MATLAB Central File Exchange. 2018. Accessed August 2, 2024. https://www.mathworks.com/matlabcentral/fileexchange/45416-surfacesmooth.

[22] Feuvret L, Noël G, Mazeron JJ, Bey P. Conformity index: a review. Int J Radiat Oncol Biol Phys 2006;64(2):333–42. https://doi.org/10.1016/j.ijrobp.2005.09.028.

[23] Wu J, Gan M, Zhang W, Jiang R. Prediction of disease-associated single amino acid polymorphisms based on physiochemical features. Int J Biosci Biochem Bioinforma 2011;1(2):102–8. https://doi.org/10.7763/ijbbb.2011.v1.19.

[24] Paolo C, Andrea Bettinelli SS. Repository for the study "Bladder Surface-based Analysis proves the dosimetric improvements of Online Adaptive Radiotherapy over Plan of the day." Zenodo. doi:10.5281/zenodo.14593384.

[25] Hafeez S, Webster A, Hansen VN, et al. Protocol for tumour-focused dose-escalated adaptive radiotherapy for the radical treatment of bladder cancer in a multicentre phase II randomised controlled trial (RAIDER): radiotherapy planning and delivery guidance. BMJ Open 2020;10(12). https://doi.org/10.1136/BMJOPEN-2020-041005.

[26] Kong V, Hansen VN, Hafeez S. Image-guided adaptive radiotherapy for bladder cancer. Clin Oncol (R Coll Radiol) 2021;33(6):350–68. https://doi.org/10.1016/J.CLON.2021.03.023.